Particle-to-fluid heat transfer in particle-laden turbulence

Hadi Pouransari and Ali Mani*
Department of Mechanical Engineering, Stanford University, Stanford, California 94305, USA

(Received 28 October 2017; published 25 July 2018)

Preferential concentration of inertial particles by turbulence is a well-recognized phenomenon. This study investigates how this phenomenon impacts the mean heat transfer between the fluid phase and the particle phase. Using direct numerical simulations of homogeneous and isotropic turbulent flows coupled with Lagrangian point particle tracking, we explore this phenomenon over a wide range of input parameters. Among the nine independent dimensionless numbers defining this problem, we show that the particle Stokes number, defined based on a large-eddy time, and an identified number called the heat-mixing parameter have the most significant effect on particle-to-gas heat transfer, while variation in other nondimensional numbers can be ignored. An investigation of regimes with significant particle mass loading suggests that the mean heat transfer from particles to gas is hardly affected by momentum two-way coupling. Using our numerical results, we propose an algebraic reduced-order model for heat transfer in particle-laden turbulence.

DOI: 10.1103/PhysRevFluids.3.074304

I. INTRODUCTION

A broad range of natural and industrial processes involve interaction of particles and background turbulent flows, e.g., formation of clouds [1,2], dispersion of pollutant in urban areas [3], planetary accretion [4], spray combustion [5], and particle-based solar receivers [6]. Particle-turbulence interaction results in a range of well-studied phenomena. A particle immersed in turbulent flow experiences a centrifugal force from high-vorticity regions toward high-strain regions. This results in an inhomogeneous distribution of particles, known as preferential concentration [7,8]. Where gravity is present particles exhibit preferential sweeping [9]. In wall-bounded particle-laden flows, turbophoresis, which refers to the tendency of particles to concentrate close to the wall, is expected [10].

In many of the particle-laden flow scenarios, a primary interest is in understanding thermal exchanges between the two phases. For example, in particle-based solar receivers, particles are the primary absorbers of external radiation, which then conductively transfer their absorbed heat to the carrier fluid. The heated particles absorb a fraction of the received flux and transfer the rest to the surrounding fluid. In this case radiation is not primarily absorbed by the gas phase since most gases are transparent to light.

In the case of heated particle-laden flows, additional phenomena are observed [11] which showed that under sufficiently large thermal flux, hot particles can modify turbulence spectra through pressure dilatation. When gravity is present, heated particles give rise to nonuniform buoyant forcing of the flow, resulting in a sustained turbulence [12,13]. Reference [14] showed that when particles are heated the preferential sweeping can be suppressed or even reversed.

In a previous study [6] we investigated a specific regime of particle-laden flows and showed that preferential concentration of particles by turbulence can adversely impact the heat-transfer

*alimani@stanford.edu

efficiency. To obtain a fundamental understanding of the impact of particle clustering on heat transfer, in the present study we consider a canonical setting involving heat transfer from inertial particles to statistically stationary homogeneous isotropic turbulent flows. By considering a combination of direct numerical simulation (DNS) data and a simple phenomenological model, we develop and verify an algebraic model for heat transfer in particle-laden turbulent flows. Turbulence in this study is maintained by a forcing mechanism [15]. We show that momentum two-way coupling between particles and the fluid does not affect the mean heat transfer between two phases.

II. MODEL PROBLEM

A. Assumptions

We consider direct numerical simulations of homogenous isotropic turbulence (HIT) laden with heated point particles in a triply periodic box with length L. The simulation code [16] is fourth order in time and second order in space using a uniform staggered grid. A linear forcing scheme [15,17] is used to maintain a statistically stationary turbulence with zero-mean velocity.

Each simulation starts with two transition stages. Collection of heat-transfer statistics is performed after these transitions when the thermal exchange process reaches a statistically stationary condition. At the first transition stage the cold mixture (with temperature T_0) is simulated for a sufficiently large time with no external heating to obtain a fully developed particle-laden turbulence. By monitoring the fluid kinetic energy and particle segregation (see, for example, [18]) versus time, we verify that a healthy particle-laden turbulence is achieved. This is achieved after 50 large-eddy turnover times defined below. The first stage is followed by the second transition stage, where particle heating is activated with constant receiving heat flux for each particle and the heated mixture is allowed to develop. The statistically stationary heated state is verified by monitoring the mean particle-to-fluid heat flux versus time. All statistics are collected after these two transition stages over a period of order 100 large-eddy turnover times. Note that when a statistically stationary state is achieved, the ensemble-average particle and fluid temperatures grow linearly with time, while the ensemble-average temperature difference and particle-to-fluid heat transfer are constant.

The fluid phase is assumed to be a variable density gas governed by the ideal gas equation of state $P = \rho R T_g$, subject to a low-Mach flow. Therefore, the thermodynamic pressure is considered to be constant in space but can change in time. The dynamic viscosity μ, constant-volume and constant-pressure specific-heat coefficients C_v and C_p, and heat conductivity coefficient k of the gas are assumed to be constant and independent of the temperature. Conservation of mass implies constant average gas density ρ_0.

Monodispersed spherical particles with density $\rho_p \gg \rho_0$ and a constant diameter d_p much smaller than the Kolmogorov microscale are suspended in the fluid. The particle specific heat coefficient C_{vp} is constant and independent of the temperature. We assume the particle temperature T_p to be a lumped quantity (constant along one particle) justified by a large particle Biot number. The slip velocity between the particle and the surrounding gas is assumed to be a finite small value. Thus, we assume that the particle momentum and heat exchange with the fluid can be expressed, respectively, in terms of drag and heat exchange laws derived in the low-Reynolds-number and low-Péclet-number limits. We ignore the convective effects at the scale of particles justified by low thermal Péclet number based on slip velocity and particle diameter.

The particle-fluid mixture is assumed to be very dilute (volume fraction $\sim 10^{-5}$). We use a simplified version of the Maxey-Riley [19] equations describing the dynamics of an immersed particle and model particle motion through the Lagrangian point particle framework. In the regimes considered in our study, Stokes drag is the only significant force experienced by particles. We ignore momentum two-way coupling (i.e., particles do not modify the fluid through the momentum equation). In Sec. III E we will revisit the impact of momentum two-way coupling on the mean heat transfer.

B. Nondimensional equations

Based on the aforementioned assumptions, we introduce a set of dimensionless equations describing heated particle-laden flows. We use the flow integral length scale $l = u_{\rm rms}^3/\epsilon$ as the reference length scale, where $u_{\rm rms}$ is the root mean square of the single-component velocity fluctuations and ϵ is the averaged dissipation rate. The large-eddy turnover time $\tau_l = l/u_{\rm rms}$ is used as the reference timescale. In addition, $u_{\rm rms}$, ρ_0, and T_0 are used to nondimensionalize velocities, gas density, and temperatures, respectively.

The conservation of mass, momentum, and energy for the gas is represented, respectively, by the set of nondimensional equations

$$\frac{\partial \rho}{\partial t} + \frac{\partial}{\partial x_j}(\rho u_j) = 0, \tag{1}$$

$$\frac{\partial}{\partial t}(\rho u_i) + \frac{\partial}{\partial x_j}(\rho u_i u_j) = -\frac{\partial p}{\partial x_i} + \frac{1}{\mathrm{Re}}\frac{\partial}{\partial x_j}\left(\frac{\partial u_i}{\partial x_j} + \frac{\partial u_j}{\partial x_i} - \frac{2}{3}\frac{\partial u_k}{\partial x_k}\delta_{ij}\right) + \frac{1}{3}\rho u_i, \tag{2}$$

$$\frac{\partial}{\partial t}(\rho T_g) + \gamma\frac{\partial}{\partial x_j}(\rho T_g u_j) = \frac{\gamma}{\mathrm{Re\,Pr}}\frac{\partial^2 T_g}{\partial x_j \partial x_j} + \sum_{i=1}^{N_p}\frac{T_{p_i} - T_g(x_{p_i})}{\sigma_l}\delta(\boldsymbol{x} - \boldsymbol{x}_{p_i}), \tag{3}$$

where ρ, u, p, and T_g denote density, velocity, hydrodynamic pressure, and temperature of the gas phase, respectively. The last term in Eq. (2) is the nondimensionalized linear forcing term [15] to maintain turbulence (with dimensionless dissipation rate 1). The last term in Eq. (3) is the heat transfer from particles to the gas. In addition, T_{p_i} and $\boldsymbol{x}_{p_i}$, respectively, represent temperature and position of a particle with index $1 \leqslant i \leqslant N_p$, where N_p is the total number of Lagrangian particles. Further, δ is the dimensionless three-dimensional Dirac delta function, which is numerically approximated using trilinear interpolation and projection.

The nondimensionalized equation of state for ideal gas is $P = \rho T_g$. The thermodynamic pressure is nondimensionalized with $\rho_0 R T_0$, where R is the gas constant. Note that, given the low-Mach-number assumption, the thermodynamic pressure is assumed to be constant in space.

Equations (4) and (5) are a set of nondimensional equations representing the kinematics, dynamics, and energy conservation for a particle p_i, respectively,

$$\frac{d}{dt}\boldsymbol{x}_{p_i} = v_{p_i}, \quad \frac{d}{dt}v_{p_i} = -\frac{v_{p_i} - u(\boldsymbol{x}_{p_i})}{\mathrm{St}_l}, \tag{4}$$

$$\chi\frac{d}{dt}T_{p_i} = \mathcal{S} - \frac{T_{p_i} - T_g(\boldsymbol{x}_{p_i})}{\sigma_l}, \tag{5}$$

where v_{p_i} denotes the velocity of a particle with index i. The first and second terms on the right-hand side of Eq. (5) are the constant heat flux absorbed by a particle and the heat transfer from the particle to the gas, respectively.

Next we introduce the dimensionless factors defined in Eqs. (1)–(5): $\mathrm{Re} = \rho_0 u_{\rm rms} l/\mu$ is the Reynolds number, $\gamma = C_p/C_v$ is the ratio of gas heat capacities, $\mathrm{Pr} = C_p\mu/k$ is the Prandtl number, and $\mathrm{St}_l = \tau_p/\tau_l$ is the particle Stokes number, which is the ratio of the particle momentum relaxation time $\tau_p = \rho_p d_p^2/18\mu$ to the gas large-eddy turnover time.

Here $\sigma_l = \tau_{th}/\tau_l$ is the heat-mixing parameter defined as the ratio of the gas thermal relaxation time $\tau_{th} = \rho_0 C_v/(\mathrm{Nu}\pi d_p k n_0)$ to the large-eddy turnover time, where $n_0 = N_p/L^3$ is the mean particle concentration and Nu is the Nusselt number for a particle-to-gas heat transfer. Note that we selected the fluid thermal relaxation time, as opposed to the commonly used particle thermal relaxation time to form the dimensionless heat-mixing parameter. For reasons that are discussed in Sec. III F, we will see that the former choice results in a minimal number of significant dimensionless parameters, while the latter choice does not.

The term $\chi = n_0 C_{vp}\rho_p \pi d_p^3/(6\rho_0 C_v)$ is the ratio of the dispersed phase total heat capacity to the gas phase total heat capacity. In addition, $\mathcal{S} = \mathcal{H} n_0 \tau_l/(T_0\rho_0 C_v)$ is the nondimensional heat source,

where $\mathcal{H}$ is the external heat flux received by each particle; $\mathcal{S}$ can be interpreted as the ratio of the large-eddy turnover time to the gas warmup time $\tau_h = T_0\rho_0 C_v/(\mathcal{H}n_0)$.

III. HEAT-TRANSFER MODEL

A. Reduced-order equations

In this section, we develop a reduced-order model to describe the evolution of the averaged particle and gas temperature. We start with the definition of the averaging operator.

For a given scalar field ψ and a weight function w in domain Ω, the weighted average of ψ is defined as

$$\langle\psi\rangle_w = \frac{\langle w\psi\rangle}{\langle w\rangle} \quad \text{where } \langle\psi\rangle = \frac{1}{\mathrm{Vol}(\Omega)}\iiint_\Omega \psi(\boldsymbol{x})d\boldsymbol{x}. \tag{6}$$

If we use the gas density ρ as the weight, $\langle\psi\rangle_\rho$ is the Favre average [20]. We define the dimensionless particle local concentration as $n(\boldsymbol{x}) = 1/N_p \sum_{i=1}^{N_p} \delta(\boldsymbol{x} - \boldsymbol{x}_{p_i})$. Therefore, $\langle\psi\rangle_n = 1/N_p \sum_{i=1}^{N_p} \psi(\boldsymbol{x}_{p_i})$ and in the case of particle temperature $\langle T_p\rangle_n = 1/N_p \sum_{i=1}^{N_p} T_{p_i}$.

To obtain reduced-order heat-transfer equations for the gas and particles, we take the average of Eqs. (3) and (5). Noting that $\langle\rho\rangle = \langle n\rangle = 1$ in the nondimensional form we get

$$\begin{aligned} \frac{d}{dt}\langle T_g\rangle_\rho &= \frac{\langle T_p\rangle_n - \langle T_g\rangle_n}{\sigma_l}, \\ \chi\frac{d}{dt}\langle T_p\rangle_n &= \mathcal{S} - \frac{\langle T_p\rangle_n - \langle T_g\rangle_n}{\sigma_l}. \end{aligned} \tag{7}$$

B. Correction factor

Equations (7) are exact but not closed due to the appearance of $\langle T_g\rangle_n$ on the right-hand sides. Similar to [6], we define a correction factor for the heat-transfer term as follows to close the equations:

$$\varphi = \frac{\langle T_p\rangle_n - \langle T_g\rangle_n}{\langle T_p\rangle_n - \langle T_g\rangle_\rho}. \tag{8}$$

Therefore, Eqs. (7) transform to the equations

$$\begin{aligned} \frac{d}{dt}\langle T_g\rangle_\rho &= \varphi\frac{\langle T_p\rangle_n - \langle T_g\rangle_\rho}{\sigma_l}, \\ \chi\frac{d}{dt}\langle T_p\rangle_n &= \mathcal{S} - \varphi\frac{\langle T_p\rangle_n - \langle T_g\rangle_\rho}{\sigma_l}, \end{aligned} \tag{9}$$

where $\langle T_g\rangle_n$ is the average gas temperature experienced by particles, similar to the concept of average gas velocity experienced by particles when the drift velocity is concerned [21]. Since particles are directly heated, it is expected that the average temperature of the gas at the location of particles is greater than the volume-average temperature of the gas $\langle T_g\rangle_n \geqslant \langle T_g\rangle_\rho$. Hence, we expect $0 \leqslant \varphi \leqslant 1$. The closure question is then to determine φ in terms of known input parameters. This is similar to the work by Sumbekova et al. [22], in which they investigated the parameter space of unheated particle-laden turbulence experimentally to explore the effect of each parameter on preferential clustering.

C. Parameter study

We investigate the dependence of the parameter φ in Eq. (9) on the dimensionless numbers governing the problem as introduced in Sec. II B. Considering common gas-solid mixtures, we assume $\gamma = 1.4$, $\mathrm{Pr} = 0.7$, and $\mathrm{Nu} = 2$. We sweep the parameter space by changing the remaining dimensionless number(s) of interest at a moment, while all other dimensionless numbers are kept

TABLE I. Nominal value of dimensionless numbers.

Parameter	Nominal value	Range
N_p	10^5	10^5 to 10^7
$\mathcal{S}$	2	1 to 10
χ	1.0	10^{-2} to 10^2
St_l	0.15	10^{-2} to 1
σ_l	0.5	10^{-2} to 10^2
Re	47	10 to 10^3

constant. In Table I we list the nominal value and sweeping range of each dimensionless number. For each dimensionless number, we run a simulation of the full three-dimensional equations for a sufficiently long time and average the value of φ when the heated HIT is developed in time by postprocessing the data to compute terms on the right-hand side of Eq. (8).

Note that we run very long simulations as a mathematical trick to compute converged statistics more easily instead of computing many simulations over a short time and then taking their average. For this we consider constant material properties. However, our data are intended to represent the much shorter evolution of ensemble-average statistics in an experiment.

The heat-transfer equations are linearly dependent on $\mathcal{S}$ and thus one expects the correction factor φ to be independent of this parameter. This expectation is justifiable as long as the thermal flux is not too strong to modify the turbulence itself [11]. Figure 1(a) depicts φ as a function of $\mathcal{S}$, while other dimensionless numbers are kept at their nominal values, verifying that φ is independent of $\mathcal{S}$. In addition, in the limit of sufficiently large N_p and negligible particle-particle collisions, it is expected that φ is independent of N_p. Figure 1(b) shows φ versus N_p confirming its independence on N_p. Increasing N_p and/or $\mathcal{S}$ gives rise to higher total heat transfer from the particles to the gas, yet the correction factor is constant.

In Fig. 1(c) we plot φ as a function of the particle-to-gas total heat capacity χ. This figure suggests a weak dependence of φ on χ, particularly in the limit of large or small χ. In Sec. III F we provide a phenomenological model justifying this observation. Therefore, only three remaining dimensionless numbers Re, St_l, and σ_l may significantly affect the correction coefficient φ.

Figure 1(d) illustrates the variation of φ as a function of Reynolds number. The bottom x axis shows Re and the top x axis shows $\mathrm{Re}_\lambda = \rho_0 u_{\mathrm{rms}} \lambda/\mu$, the Reynolds number based on the Taylor

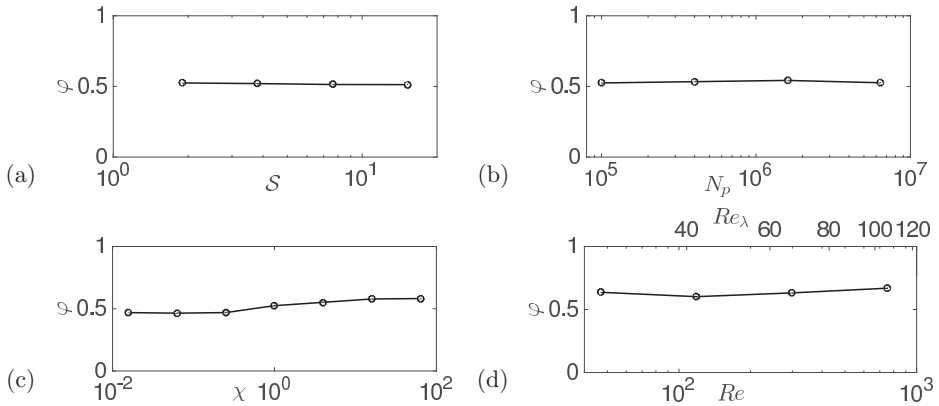

FIG. 1. Correction factor φ as a function of (a) total number of particles N_p, (b) nondimensional heat flux $\mathcal{S}$, (c) particle-to-gas heat capacity ratio χ, and (d) Reynolds number Re and Re_λ.

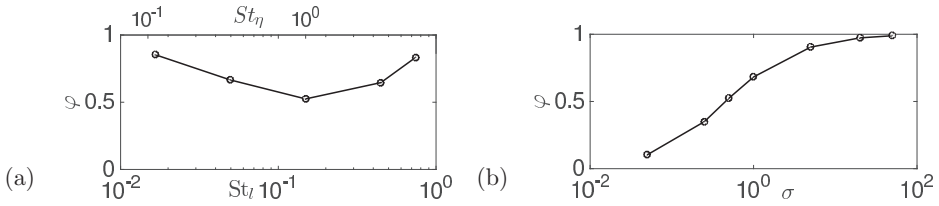

FIG. 2. Correction factor φ as a function of (a) Stokes number St_l and St_η and (b) heat-mixing parameter σ_l.

microscale. For HIT we have $\mathrm{Re} = \mathrm{Re}_\lambda^2/15$. The values of other dimensionless numbers are the same as in Table I, except for the particle Stokes number, which is kept at $\mathrm{St}_l = 0.06$. Our results suggest that when the Stokes number and heat-mixing parameter are defined based on the large-eddy turnover time, φ is a weak function of the Reynolds number. We further discuss implications of alternative choices of reference timescale in the definition of Stokes number and heat-mixing parameter in Sec. III D.

Note that we found the correction factor φ to be independent of N_p, $\mathcal{S}$, and χ assuming no turbulence modification by the particles. In general, particles can modify the background turbulence either through the momentum exchange or through local expansion resulting from heat transfer. The former is significant when the particle mass loading ratio is high [23–25] and the latter is significant in the case of high heating that results in high dilatational modes quantified by $|\tau_l \nabla \cdot u|$ [11]. This is the case in most turbulent combustion applications, for example. All of the investigated cases are indeed in the regime where the dilatation due to heating is small compared to the large-eddy turnover time. However, the mass loading ratio is significant in some cases. We show in Sec. III E that although turbulence modulation by particles can be considerable in these cases, the impact on the mean heat transfer is negligible.

In Fig. 2(a) the heat-transfer correction factor is plotted as a function of particle Stokes number. The bottom x axis is the Stokes number based on the large-eddy turnover time St_l and the top x axis shows the Stokes number based on the Kolmogorov timescale $\mathrm{St}_\eta = \tau_p/\tau_\eta$. For HIT we have $\mathrm{St}_\eta = \sqrt{\mathrm{Re}}\mathrm{St}_l$.

For very small and large Stokes numbers the particle distribution is close to homogeneous. Therefore, the weights in Eq. (6) are almost uniform and φ is close to one. For moderate values of Stokes number the highest level of preferential concentration is expected. In this case the particle-to-gas heat transfer occurs at the location of particle clusters that inevitably introduce spatial heterogeneity. Hence, when preferential concentration is high, the effective volume of cold gas experienced by the particles is reduced, resulting in less heat transfer from the particles to the gas (i.e., $\varphi < 1$).

Figure 2(b) shows φ as a function of the heat-mixing parameter σ_l. Here φ is a strictly increasing function of σ_l such that as $\sigma_l \to \infty$, $\varphi \to 1$, and as $\sigma_l \to 0$, $\varphi \to 0$. The value of σ_l quantifies the rate of heat mixing by turbulence in terms of the gas thermal relaxation timescale. Small values of σ_l means that the heat mixing due to turbulence is weak, and large values of σ_l represent strong heat mixing due to turbulence. We study the effects of simultaneous variations of St_l and σ_l in Sec. III F.

D. Choice of reference timescale

In this study we use the large-eddy turnover time as the flow reference timescale. Alternatively, we could use the Kolmogorov timescale as the reference flow timescale. Using the Kolmogorov timescale, in particular, is appealing in order to define the Stokes number as done in numerous previous studies characterizing particle preferential concentration.

In Fig. 1(d) we showed that the correction factor φ has a small dependence on the Reynolds number, whereas all other nondimensional numbers are kept constant. Note that as the Reynolds

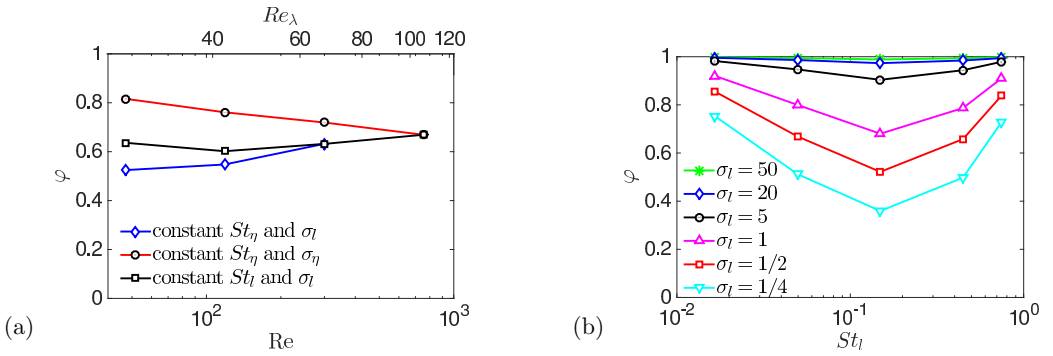

FIG. 3. Variation of φ as a function of (a) Reynolds number when the Stokes number and heat-mixing parameter are kept constant, where the subscripts η and l refer to normalizing by Kolmogorov and large-eddy turnover times, respectively, $\mathrm{St}_l = \tau_p/\tau_l$, $\mathrm{St}_\eta = \tau_p/\tau_\eta$, $\sigma_l = \tau_{th}/\tau_l$, and $\sigma_\eta = \tau_{th}/\tau_\eta$, and (b) heat-mixing parameter σ_l and Stokes number St_l.

number increases, the ratio between the large-eddy turnover time and the Kolmogorov time increases as well. Therefore, the choice of reference timescale for the Stokes number and the heat-mixing parameter, which are kept constant while the Reynolds number is varied, is important.

In Fig. 3(a) variation of φ with Reynolds number is shown when different flow timescales are used for defining the Stokes number and/or heat-mixing parameter σ. The subscript l denotes normalizing with the large-eddy turnover time and the subscript η denote normalizing with the Kolmogorov time. Figure 3(a) demonstrates that our choice of large-eddy turnover time for both the Stokes number and heat-mixing parameter results in the lowest dependence of φ on Reynolds. Further studies are required to investigate variations of φ for much larger values of Reynolds number.

E. Effect of momentum two-way coupling

In all the cases considered above, momentum two-way coupling between the particles and gas is ignored in the simulations to simplify the analysis of the system. However, for significant mass loading ratios the momentum exchange between the two phases can modify the turbulence dynamic.

To verify the validity of the results presented here, we ran a simulation of the nominal case (see Table I) with consideration of momentum two-way coupling between the particles and gas [24]. Similar to the heat exchange between two phases, we use a trilinear interpolation and projection for numerical calculation of the momentum exchange. The correction factor φ for the nominal case changes from 0.525 to 0.526 when momentum two-way coupling is considered. This shows that the effect of momentum two-way coupling is negligible on the correction factor introduced here.

F. Closure model

We concluded that the Stokes number and heat-mixing parameter, defined based on τ_l, are the most relevant dimensionless numbers determining φ. Therefore, we sweep the parameter space in two dimensions (St_l and σ_l) to discover the full dependence of φ on the input parameters. In Fig. 3(b) variation of φ as a function of Stokes number is plotted for different values of σ_l. Other dimensionless numbers are kept at their nominal values as reported in Table I.

The nonmonotonic dependence of φ as a function of St_l can be observed for all values of σ_l. However, as $\sigma_l \to \infty$ the dependence of φ on the particle Stokes number vanishes. For large values of σ_l the heat mixing due to turbulence is strong; therefore, even for a high level of preferential concentration the heat transferred from the particles to the gas is quickly mixed uniformly. This fast mixing makes the gas temperature uniform despite the heterogeneity of the source and thus brings $\langle T_g \rangle_n$ closer to $\langle T_g \rangle_\rho$, leading to $\varphi \simeq 1$. This effect is visually evident in Fig. 4, where the

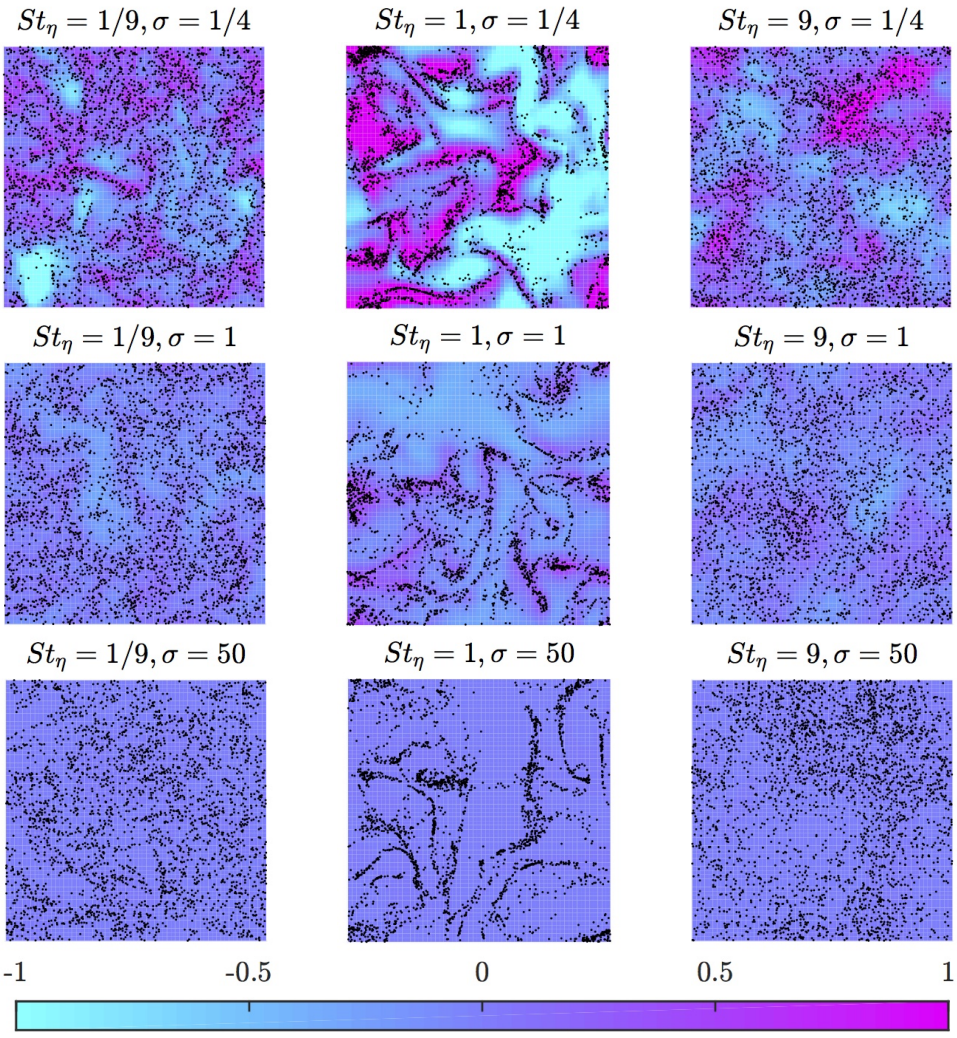

FIG. 4. Particle distribution and normalized fluid temperature deviation $T_g - \langle T_g \rangle_\rho$ contours for different combinations of St_η and σ_l in one slice of the domain.

particle distribution and normalized fluid temperature deviations $T_g - \langle T_g \rangle_\rho$ are illustrated for various combinations of St_η and σ_l. Note that particles have a high level of preferential concentration when $\mathrm{St}_\eta \sim O(1)$ irrespective of the value of σ_l (the middle column in Fig. 4). However, only for small values of σ_l the particle preferential concentration affects the particle-to-gas heat transfer.

Here we introduce a simple phenomenological heat-transfer model consistent with the observed dependence of φ on the dimensionless parameters. We use the result of this approach to provide a closed algebraic form for the correction coefficient φ.

Consider the cloud of gas in the vicinity of particles as shown in Fig. 5(a). Assume that this cloud occupies the volume fraction f of the total gas. The coefficient $0 \leqslant f \leqslant 1$ is only a function of the particle spatial distribution and thus $f = f(\mathrm{St}_l)$. In this approach we consider one averaged temperature for the cloud of gas near the particles (gas 1) and one for the rest of the gas (gas 2), denoted by T_{g_1} and T_{g_2}, respectively. We assume that particles receive energy from an external heat source and transfer energy conductively to the surrounding cloud of gas. This cloud then transfers

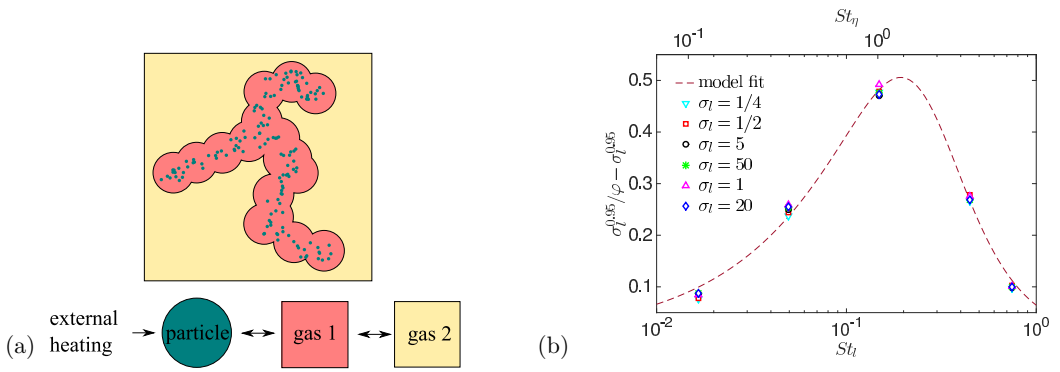

FIG. 5. (a) Particle-to-gas heat-transfer model schematics and (b) collapse of $\sigma_l{}^p/\varphi - \sigma_l{}^p$ versus St_l for different values of σ_l, with $p = 0.95$.

heat convectively to the rest of the gas. In the former, the heat transfer is dominated by the gas thermal relaxation time τ_{th} augmented by a factor f to account for the smaller mass fraction. In the latter, the large-eddy turnover time τ_l is the dominant timescale in the heat transfer as the mixing by large eddies is the main heat-transfer mechanism (see [26–28]). Using the same nondimensionalization as in Sec. II B, the governing equations are

$$\begin{aligned} \chi \frac{d}{dt}\langle T_p\rangle_n &= -\frac{1}{\sigma_l}(\langle T_p\rangle_n - T_{g_1}) + \mathcal{S}, \\ f\frac{d}{dt}T_{g_1} &= \frac{1}{\sigma_l}(\langle T_p\rangle_n - T_{g_1}) - (T_{g_1} - T_{g_2}), \\ (1-f)\frac{d}{dt}T_{g_2} &= (T_{g_1} - T_{g_2}). \end{aligned} \tag{10}$$

Neglecting spatial variation of the gas density, we can write

$$\langle T_g\rangle_\rho = fT_{g_1} + (1-f)T_{g_2}. \tag{11}$$

Combining Eqs. (10) and (11) and noting that under the fully developed conditions all temperatures increase linearly with time with the same slope [$=\mathcal{S}/(\chi+1)$, to satisfy conservation of energy for the full system], we can derive the following equation:

$$\chi\frac{d}{dt}\langle T_p\rangle_n = \mathcal{S} - \frac{\sigma_l}{\sigma_l + (1-f)^2}\frac{\langle T_p\rangle_n - \langle T_g\rangle_\rho}{\sigma_l}. \tag{12}$$

A comparison against Eq. (9) suggests that the correction factor φ introduced in Eq. (8) is $\varphi = \sigma_l/[\sigma_l + (1-f)^2]$. This analysis also provides insight into the observed weak dependence of φ on χ, as the derived expression does not involve the parameter χ in this simplified limit.

Next, assuming that f is only a function of St_l, we consider a generalized form for $\varphi = \sigma_l{}^p/[\sigma_l{}^p + g(\mathrm{St}_l)]$. Based on our phenomenological model, we expect a value of p close to 1. Reverse engineering of this expression indicates that $\sigma_l{}^p/\varphi - \sigma_l{}^p$ versus St_l must result in plots independent of σ_l. As shown in Fig. 5(b), $p = 0.95$ results in collapse of curves corresponding to different values of σ_l, confirming the usefulness of our phenomenological model.

We consider $g(\mathrm{St}_l) = \alpha\mathrm{St}_l^{\eta_1}/(\mathrm{St}_l^{\eta_2} + \beta)$ as a generalization of the expression suggested by Esmaily-Moghadam and Mani [29] to quantify the level of particle preferential concentration. We

found the optimal values of $\alpha = 0.066$, $\beta = 0.025$, $\eta_1 = 0.8$, and $\eta_2 = 2.8$ by fitting φ to our data [see the dashed line in Fig. 5(b)]. Finally, we propose the following algebraic form for the particle-to-gas heat-transfer correction coefficient:

$$\varphi = \frac{{\sigma_l}^{0.95}}{{\sigma_l}^{0.95} + 0.066 \frac{\mathrm{St}_l^{0.8}}{\mathrm{St}_l^{2.8} + 0.025}}. \tag{13}$$

IV. CONCLUSION

In this paper, we developed a nondimensional set of equations describing heated point particles suspended in a variable-density turbulent flow. We studied the averaged particle-to-fluid heat transfer using direct numerical simulations for fluid and Lagrangian point particle tracking for the dispersed phase. In the presented formulation, nine nondimensional numbers appear. Considering a wide range of applications involving small solid particles in gas, we investigated the regime in which $\gamma = 1.4$, $\mathrm{Pr} = 0.7$, and $\mathrm{Nu} = 2$, while we systematically varied all other nondimensional numbers.

We showed that in the regimes where the dilatational time is not fast compared to the eddy time the number of particles, the dimensionless heating rate, the ratio of particle-to-fluid heat capacities, and the Reynolds number have a minor effect on the mean heat-transfer coefficient. However, our results indicate that the particle Stokes number St_η and the introduced nondimensional number, the heat-mixing parameter σ_l, have a significant effect on the particle-to-fluid heat transfer. The former parameter governs the topology of the particle distribution, which controls the spatial distribution of heat sources to the fluid. The latter parameter determines how fast the background fluid can mix the heat received by particles compared to the gas nominal thermal relaxation time. Therefore, even for a high level of preferential concentration, we can expect an almost uniform fluid temperature distribution due to turbulent mixing when σ_l is high.

Using our parameter study, in Sec. III F we introduced an algebraic closure formula to model the macroscopic particle-to-gas heat transfer for general conditions. The inputs of our model are St_l and σ_l, which were found to be the most relevant nondimensional numbers for the particle-to-fluid heat transfer. This result can be used as a map predicting the order of magnitude of heat-transfer modification in general configurations.

Furthermore, we explored different timescales to define the Stokes number and heat-mixing parameter, namely, the large-eddy turnover time and Kolmogorov time. Our results indicate that macroscopic-averaged heat-transfer correction coefficient φ is best described by these parameters (i.e., independent of the system Reynolds number) when they are nondimensionalized based on the large-eddy time. Investigation of cases with and without momentum two-way coupling between the two phases suggests that the macroscopic heat-transfer correction coefficient φ is insensitive to modulation of turbulence by the particles.

A future application of this study would be to provide closure to heat-transfer terms in subgrid-scale models that do not directly capture particle clustering. For example, Reynolds-averaged Navier-Stokes models only represent the ensemble-average velocity fields. Therefore, even the most accurate particle solver can provide the mean particle number density while missing the clustering effect. This is a suitable situation for application of the proposed model, by which the heat-transfer terms can be closed using the available mean particle number density and mean turbulence dissipation rate (provided by the turbulence model). Future research can investigate whether the presented approach can be adopted in the context of large-eddy simulations, where the input parameters are defined based on the subgrid turbulence dissipation rate.

This work can be extended by relaxing some of our assumptions such as considering temperature-dependent thermodynamical properties, inhomogeneous flows, and compressibility effects in the case of extreme heating. Furthermore, the dependence of our model parameter φ on the Reynolds number can be further studied by considering flows with larger values of Reynolds number.

ACKNOWLEDGMENTS

We would like to acknowledge support from the U.S. Department of Energy, DE-NA0002373 under the Predictive Science Academic Alliance Program 2 at Stanford University.

[1] R. A. Shaw, Particle-turbulence interactions in atmospheric clouds, Annu. Rev. Fluid Mech. **35**, 183 (2003).
[2] W. W. Grabowski and L.-P. Wang, Growth of cloud droplets in a turbulent environment, Annu. Rev. Fluid Mech. **45**, 293 (2013).
[3] R. E. Britter and S. R. Hanna, Flow and dispersion in urban areas, Annu. Rev. Fluid Mech. **35**, 469 (2003).
[4] J. N. Cuzzi, R. C. Hogan, J. M. Paque, and A. R. Dobrovolskis, Size-selective concentration of chondrules and other small particles in protoplanetary nebula turbulence, Astrophys. J. **546**, 496 (2001).
[5] S. Sahu, Y. Hardalupas, and A. M. K. P. Taylor, Droplet-turbulence interaction in a confined polydispersed spray: Effect of droplet size and flow length scales on spatial droplet-gas velocity correlations, J. Fluid Mech. **741**, 98 (2014).
[6] H. Pouransari and A. Mani, Effects of preferential concentration on heat transfer in particle-based solar receivers, J. Solar Energy Eng. **139**, 021008 (2017).
[7] B. J. Lazaro and J. C. Lasheras, Particle dispersion in a turbulent, plane, free shear layer, Phys. Fluids A **1**, 1035 (1989).
[8] K. D. Squires and J. K. Eaton, Preferential concentration of particles by turbulence, Phys. Fluids A **3**, 1169 (1991).
[9] L.-P. Wang and M. R. Maxey, Settling velocity and concentration distribution of heavy particles in homogeneous isotropic turbulence, J. Fluid Mech. **256**, 27 (1993).
[10] M. W. Reeks, The transport of discrete particles in inhomogeneous turbulence, J. Aerosol Sci. **14**, 729 (1983).
[11] H. Pouransari, H. Kolla, J. H. Chen, and A. Mani, Spectral analysis of energy transfer in turbulent flows laden with heated particles, J. Fluid Mech. **813**, 1156 (2017).
[12] R. Zamansky, F. Coletti, M. Massot, and A. Mani, Radiation induces turbulence in particle-laden fluids, Phys. Fluids **26**, 071701 (2014).
[13] R. Zamansky, F. Coletti, M. Massot, and A. Mani, Turbulent thermal convection driven by heated inertial particles, J. Fluid Mech. **809**, 390 (2016).
[14] A. Frankel, H. Pouransari, F. Coletti, and A. Mani, Settling of heated particles in homogeneous turbulence, J. Fluid Mech. **792**, 869 (2016).
[15] C. Rosales and C. Meneveau, Linear forcing in numerical simulations of isotropic turbulence: Physical space implementations and convergence properties, Phys. Fluids **17**, 095106 (2005).
[16] H. Pouransari, M. Mortazavi, and A. Mani, Parallel variable-density particle-laden turbulence simulation, Center for Turbulence Research annual research brief, 2015 (unpublished), pp. 43–54.
[17] T. S. Lundgren, Center for Turbulence Research annual research brief, 2003 (unpublished), pp. 461–473.
[18] A. Vié, H. Pouransari, R. Zamansky, and A. Mani, Particle-laden flows forced by the disperse phase: Comparison between Lagrangian and Eulerian simulations, Int. J. Multiphase Flow **79**, 144 (2016).
[19] M. R. Maxey and J. J. Riley, Equation of motion for a small rigid sphere in a nonuniform flow, Phys. Fluids **26**, 883 (1983).
[20] D. C Wilcox, *Turbulence Modeling for CFD* (DCW Industries, La Cañada, 1998), Vol. 2.
[21] J. Jung, K. Yeo, and C. Lee, Behavior of heavy particles in isotropic turbulence, Phys. Rev. E **77**, 016307 (2008).
[22] S. Sumbekova, A. Cartellier, A. Aliseda, and M. Bourgoin, Preferential concentration of inertial sub-Kolmogorov particles: The roles of mass loading of particles, Stokes numbers, and Reynolds numbers, Phys. Rev. Fluids **2**, 024302 (2017).
[23] K. D. Squires and J. K. Eaton, Particle response and turbulence modification in isotropic turbulence, Phys. Fluids A **2**, 1191 (1990).

[24] S. Elghobashi and G. C. Truesdell, On the two-way interaction between homogeneous turbulence and dispersed solid particles. I: Turbulence modification, Phys. Fluids A **5**, 1790 (1993).
[25] S. Sundaram and L. R. Collins, A numerical study of the modulation of isotropic turbulence by suspended particles, J. Fluid Mech. **379**, 105 (1999).
[26] L. Prandtl, Bericht uber untersuchungen zur ausgebildeten turbulenz, Z. Angew Math. Phys. **5**, 136 (1925).
[27] P. E. Dimotakis, Turbulent mixing, Annu. Rev. Fluid Mech. **37**, 329 (2005).
[28] J. C. Vassilicos, Dissipation in turbulent flows, Annu. Rev. Fluid Mech. **47**, 95 (2015).
[29] M. Esmaily-Moghadam and A. Mani, Analysis of the clustering of inertial particles in turbulent flows, Phys. Rev. Fluids **1**, 084202 (2016).